Improved Chiral Photoelectron Spectroscopy via Selection of Chirality-Selective Molecular Axis Orientations: A Theoretical Analysis of Non-Negative Smooth Functions

Yoshi-Ichi Suzuki*
School of Medical Technology, Health Sciences University of Hokkaido, 1757 Kanazawa, Tobetsucho, Ishikari, Hokkaido 061-0293, Japan

(Received 24 November 2022; accepted 17 March 2023; published 7 April 2023)

Photoelectron spectroscopy for chiral discrimination is routinely performed for low photoelectron kinetic energies (PKEs), whereas it is considered impossible for high PKEs. We demonstrate theoretically that chiral photoelectron spectroscopy for high PKEs is possible using chirality-selective molecular orientation. The photoelectron angular distribution associated with one-photon ionization by unpolarized light can be characterized by a single parameter, β. We show that most other anisotropy parameters are zero when β is 2, as is often the case in the high PKEs. Exceptionally, odd-order anisotropy parameters are increased by a factor of 20 by orientation, even for high PKEs.

DOI: 10.1103/PhysRevLett.130.143202

The intensity of photoelectrons in the forward and backward light propagation directions will differ in the case of chiral molecules ionized by circularly polarized light [1–3]. This difference tends to go to zero with increasing electron energy [4], even though a high electron energy is important for the chiral resolution of ions based on electron recoil [3,5] and for liquid samples [6–9]. Interestingly, there are a few exceptions to this rule [10–12], and a reduced effect of molecular chirality appears to be inconsistent with electron diffraction phenomena such as the Cohen-Fano effect [13,14] and the focusing effect [15,16] occurring at a photoelectron energy of several hundred electron volts. This raises the question of what form the photoelectron angular distribution (PAD) takes at high energies.

In the case that randomly oriented molecules are ionized by unpolarized light, the PAD can be expressed by the asymmetry parameter [17] $\beta(-1 \le \beta \le 2)$. It has been confirmed that the value of β is typically between 1 and 2 for photoelectrons having kinetic energies on the order of 100 eV [9,18]. This is not strange because a positive β means that electrons move along the electric field of light. However, when $\beta = 2$ the electron is never emitted along the photon k vector. No intensity after rotational averaging means no intensity before averaging because the PAD function is positive. In this Letter, we show that additional parameters associated with light polarization and molecular alignment can be classified into three categories. If β is close to 2, the upper bounds of the magnitudes of the first and second categories are proportional to $(2-\beta)$ and $\sqrt{2-\beta}$, respectively. They vanish when $\beta = 2$. Importantly, the very few parameters in the third category are not correlated with β. Some of them are related to the chirality-selective molecular axis orientation [19–26], and we illustrate the magnitudes of this effect for hydrogen peroxide and methyloxirane.

The effects of polarization and multiphoton processes on PADs have been extensively studied [1,2,27–42]. In particular, the irreducible tensor theory is well suited to the evaluation of geometrical factors associated with the perturbation regime [34–42]. The PAD can typically be expanded using the statistical tensor for light, ρ_{LM}, and spherical harmonics with angles θ and φ as

$$\frac{d\sigma}{d\Omega} = \sum_{L}^{2N} c_L \sum_{M} \rho_{LM} Y_{LM}(\theta, \varphi), \tag{1}$$

where N is the number of photons and θ is the angle between the photoelectron k vector and the laboratory z' axis. This formula can be regarded as a generalization of Yang's theorem [43] to account for light polarization [44] and odd L [1,2,35] and some conclusions can be drawn without knowing the details of c_L. Note that the c_L are scalar. For one-photon or resonant two-photon ionization with the electric dipole approximation, the statistical tensor is symmetrical under space inversion. Therefore, the c_L with odd L are antisymmetric for space inversion. For these pseudoscalars to be nonzero, the system must lose inversion symmetry prior to ionization, as occurs in the case of chiral molecules. In addition, assuming the Hermiticity of the irreducible tensor [45,46], $\rho^*_{LM} = (-1)^M \rho_{L,-M}$, it follows that the sum over $\pm M$ will be a real number, and hence the c_L are real. Furthermore, there remains a requirement for Eq. (1) to be positive for *all* angles. This problem is rarely solved except in limited cases such as two-photon ionization with linearly polarized light [27].

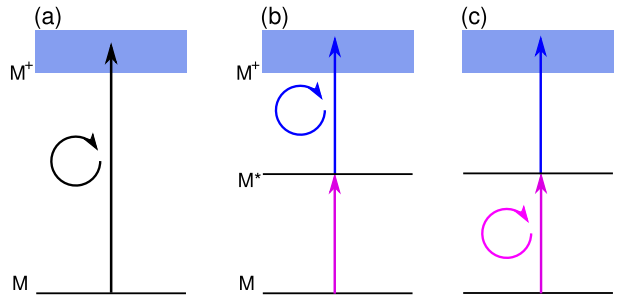

FIG. 1. Diagrams summarizing (a) one-photon ionization and resonance-enhanced two-photon ionization using circular polarization for (b) bound-free and (c) bound-bound transitions. Another photon for (b) and (c) is assumed to be unpolarized.

Alternatively, we can consider two cases for Eq. (1) to be positive. The first case assumes non-negativity of the photoelectron intensity at a *specific* angle θ_0

$$\left.\frac{d\sigma}{d\Omega}\right|_{\theta=\theta_0} \geq 0. \tag{2}$$

The second is the smoothness at angles at which the photoelectron intensity is zero. For Eq. (1) to be smooth around these angles while still being non-negative, the first derivative must have a value of zero. That is,

$$\left.\frac{d\sigma}{d\Omega}\right|_{\theta=\theta_0} = 0, \tag{3a}$$

$$\left.\frac{\partial}{\partial\theta}\frac{d\sigma}{d\Omega}\right|_{\theta=\theta_0} = 0. \tag{3b}$$

As discussed below, Eq. (2) indicates linear relationships between β and other parameters, and the two parametric functions [Eqs. (3a) and (3b)] (both of which are dependent on the scattering angle θ_0) implicitly define these relationships. Whether these conditions are sufficient or not is assessed by performing numerical calculations. We here consider one-photon and resonant two-photon ionization processes. In particular, we examine the case in which one of the photons is circularly polarized (Fig. 1), which breaks the forward-backward symmetry. We also assume that the intermediate electronic states are nondegenerate and that both the bound-bound transition and the bound-free transition can be treated using the electrical dipole approximation.

During resonant multiphoton ionization, molecules align as a result of bound-bound transitions [29,30,47]. This process is typically represented using the alignment parameters A_K, and so we rewrite Eq. (1) using these terms. The angular distribution of the molecular z axis takes $P(\theta') = \sum_{K=0}^{2} A_K P_K(\cos\theta')$, where, θ' is the angle with the laboratory z' axis and $P_K(x)$ are Legendre polynomials. An important aspect of A_K is that even if the polarization at the bound-bound transition is fixed, we can use rotational coherence [24,47] to control each of A_1 and A_2 individually, either positively or negatively.

Using A_K, the irreducible tensors are defined as

$$\rho_{LM}^{(K,k_\gamma)} = \sum_{q_\gamma} (-1)^{L-M} \begin{pmatrix} K & L & k_\gamma \\ 0 & -M & q_\gamma \end{pmatrix} A_K \rho_{k_\gamma q_\gamma}, \tag{4}$$

where $\rho_{k_\gamma q_\gamma}$ is the statistical tensor for light polarization of ionization. For circularly polarized light, $\rho_{00} = (1/\sqrt{3})$, $\rho_{10} = (-1/\sqrt{2})s_3$, $\rho_{20} = (1/\sqrt{6})$, and $|s_3| \leq 1$. Here, s_3 is a Stokes parameter indicating the degree of circular polarization and can be positive or negative, while it is physically impossible to control ρ_{20} independently of ρ_{00}. Assuming that A_K is real and $\rho^*_{k_\gamma,q_\gamma} = (-1)^{q_\gamma}\rho_{k_\gamma,-q_\gamma}$, we can prove that the composite tensors are Hermitian or anti-Hermitian depending on whether the sum $p_A = K + L + k$ is even or odd, respectively:

$$\rho_{LM}^{(K,k_\gamma)*} = (-1)^{p_A+M}\rho_{L,-M}^{(Kk_\gamma)}. \tag{5}$$

In addition, the axially symmetric components ($M = 0$) of anti-Hermitian tensors ($p_A =$ odd) disappear, due to the $3j$ symbol in Eq. (4).

For one- and two-photon ionizations, we suppose that

$$\frac{d\sigma}{d\Omega} = \sum_{KLk_\gamma} b_L^{(K,k_\gamma)} \sum_M \rho_{LM}^{(K,k_\gamma)} Y_{LM}(\theta,\varphi), \tag{6}$$

instead of Eq. (1). Here, coefficients $b_L^{(K,k_\gamma)}$ describe photoionization dynamics. They are real (purely imaginary) when the tensor $\rho_{LM}^{(K,k_\gamma)}$ is Hermitian (anti-Hermitian), due to Eq. (5). Assuming randomly oriented ensemble ($A_1 = A_2 = 0$) and linear polarization ($\rho_{20}/\rho_{00} = -\sqrt{2}$), we can show $\beta = -\sqrt{2}b_2^{(0,2)}/b_0^{(0,0)}$ by comparing Eq. (6) with $1 + \beta P_2(\cos\theta)$. We do not need to know the details about the coefficients. For example, if we demand that $1 + \beta P_2(\cos\theta) \equiv (1+\beta)\cos^2\theta + (1-\beta/2)\sin^2\theta \geq 0$ at angles 0° and 90°, we get $-1 \leq \beta \leq 2$ without knowing the physical meaning of β.

According to the $3j$ symbol in Eq. (4), $|K - k_\gamma| \leq L \leq K + k_\gamma$, and there are 17 coefficients other than $b_0^{(0,0)}$ and $b_2^{(0,2)}$. They can be grouped into 12 sets according to the parities of L and p_A and the three possible values of K. As a result, most sets consist of only one or two elements. The appearance and disappearance of each set in Eq. (6) can be controlled by the parameters of alignment and light polarization.

For example, only $b_1^{(0,1)}$ appears in the one-photon ionization of chiral molecules [1–3]. The effect of circular polarization in the ionization scheme of Fig. 1(b), which has been studied in detail by Goetz *et al.* [48], is related to $(b_1^{(2,1)}, b_3^{(2,1)})$. By breaking axial symmetry, we can observe the coefficients with odd p_A. Dubs *et al.* have shown that $b_2^{(2,1)}$ appears for aligned molecules [49], regardless of

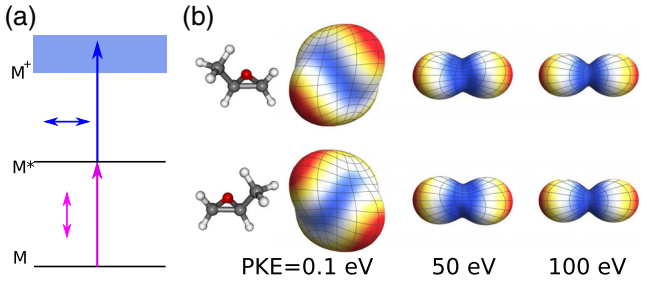

FIG. 2. (a) Scheme of linearly polarized two-photon ionization. (b) Calculated 3D polar plots of PADs of *R*- and *S*-methyloxirane (molecular orbital 14*a*), as a function of photoelectron kinetic energy (PKE). We assumed that the direction of the light is upward, the polarization of the bound-free transition is horizontal and orthogonal to the polarization of the bound-bound transition, and its transition dipole moment is parallel to the *c* axis of the moment of inertia.

molecular chirality. Hansen and Berry pointed out that chiral molecules can be detected with nonparallel linearly polarized two photons [35], using $b_1^{(2,2)}$ and $b_3^{(2,2)}$. Interestingly, the PAD depends on the chirality even with orthogonal polarizations, as shown in Fig. 2 for the 14*a* orbital of methyloxirane. This is because the function $Y_{32}(\theta,\varphi)+Y_{3,-2}(\theta,\varphi)$ is totally symmetric for the point group D_2 of this system. Figure 2 also shows that the difference in PADs between a chiral molecule and its mirror image decreases with increasing energy, even without using circularly polarized light.

On the other hand, only two sets consist of more than two elements; one is related to the ionization scheme of Fig. 1(c) and comprises $(b_1^{(1,0)}, b_1^{(1,2)}, b_3^{(1,2)})$ while the other comprises $(b_0^{(2,2)}, b_2^{(2,0)}, b_2^{(2,2)}, b_4^{(2,2)})$. The latter is a common parameter set that appears in two-photon ionization induced by linearly polarized light [50]. Both sets include the coefficients with $k_\gamma = 0$, $b_L^{(L,0)}$, which can be observed in the polarization-averaged PAD [51,52] and expected to have significant value even at high photoelectron kinetic energies [52].

Before considering individual situations, we will develop a general theory for the first and second cases. The k vector of the photon for bound-free transition is assumed to be in the $x'z'$ plane of the laboratory frame and at an angle θ_γ with respect to the z' axis. Below, δ_X and ε_Y are used as linear combinations of coefficients $b_L^{(K,k_\gamma)}$. For the sake of simplicity, we will assume that the coefficients $b_L^{(K,k_\gamma)}$ are normalized so that $b_0^{(0,0)} = 1$. We consider the angle at which the photoelectron intensity is expected to be minimal. That is $\theta = \theta_\gamma$ when $\beta = 2$. Using $Y_{LM}(\theta,\varphi)$'s explicit form and $\vartheta = \theta - \theta_\gamma$, Eq. (6) becomes

$$\frac{d\sigma}{d\Omega} \propto \Delta + \frac{3}{2}\beta\vartheta^2 + \delta + 2\varepsilon\vartheta + O(\vartheta^2), \tag{7}$$

for small angle ϑ and $\varphi = 0$, where $\Delta = 2 - \beta$. δ and ε depend on A_K, s_3, and θ_γ. Explicitly, $\delta = -\sqrt{6}s_3\delta_X$ and $\delta_X = b_1^{(0,1)}$ for Fig. 1(a) and

$$\delta = \sqrt{6}A_2 s_3 P_2(\cos\theta_\gamma)\delta_X, \tag{8}$$

$$\varepsilon = 3\sqrt{3}A_2 s_3 \sin(2\theta_\gamma)(\varepsilon_Y - \sqrt{6}\delta_X), \tag{9}$$

$$\delta_X = (\sqrt{2}b_1^{(2,1)} - \sqrt{3}b_3^{(2,1)})/\sqrt{5}, \tag{10}$$

$$\varepsilon_Y = (\sqrt{3}b_1^{(2,1)} + \sqrt{2}b_3^{(2,1)})/\sqrt{5} \tag{11}$$

for Fig. 1(b). As for the first case, Eq. (2) can be simply expressed as

$$\Delta + \delta \geq 0. \tag{12}$$

This equation gives both the upper and lower bounds of δ_X because δ becomes positive or negative [Eqs. (8) and (10)], as in A_1, A_2, and s_3. Note that these δ_X terms correspond to the first kind. For instance, we have $|b_1^{(0,1)}| \leq \Delta/\sqrt{6}$ for one-photon ionization, and $b_1^{(0,1)}$ is of the first kind.

With regard to the second case, using Eq. (7), Eqs. (3a) and (3b) become $\Delta = 0$ and $\varepsilon = 0$, respectively. To get the relation between Δ and ε, we suppose that Eqs. (3a) and (3b) hold continuously near $\vartheta = 0$, i.e.,

$$\Delta + \frac{3}{2}\beta\vartheta^2 + \delta + 2\varepsilon\vartheta = 0, \tag{13a}$$

$$3\beta\vartheta + 2\varepsilon = 0, \tag{13b}$$

resulting in $\varepsilon^2 = 3\Delta + 3\delta + O(\Delta^2)$. This equation defines the boundary of the physically possible region corresponding to the two-dimensional space of (β,ε). Positivity of PAD determines which side is possible. Thus, assuming δ can be positive and negative, we have

$$|\varepsilon| \leq \sqrt{3\Delta - 3|\delta|} \leq \sqrt{3\Delta}. \tag{14}$$

This is a general formula derived from the second case, and these ε_Y embedded in ε [Eqs. (9) and (11)] are of the second kind.

In this manner, the coefficients $b_L^{(K,k_\gamma)}$ can be categorized into three types regardless of molecular chirality or circular polarization. A complete list (Tables S1 and S2) and calculations for N_2 (Fig. S1) are provided in the Supplemental Material [53].

Because there are two equations, Eqs. (12) and (14), we can expect that most coefficients $b_L^{(K,k_\gamma)}$ are zero at $\beta = 2$. The coefficients with odd L in Figs. 1(a), 1(b), and 2 are exactly the case. For Fig. 1(b), we have

$$|\sqrt{2}b_1^{(2,1)} - \sqrt{3}b_3^{(2,1)}|/\sqrt{5} \le \frac{\Delta}{\sqrt{6}}, \tag{15}$$

$$|\sqrt{3}b_1^{(2,1)} + \sqrt{2}b_3^{(2,1)}|/\sqrt{5} \le \frac{2}{\sqrt{3}}\sqrt{\Delta}, \tag{16}$$

and hence the effect of molecular chirality disappears when $\beta = 2$. In contrast, as for Fig. 1(c), we have

$$\left|\sqrt{\frac{2}{3}}b_1^{(1,0)} - \sqrt{\frac{2}{15}}b_1^{(1,2)} + \frac{1}{\sqrt{5}}b_3^{(1,2)}\right| \le \frac{\Delta}{\sqrt{6}}, \tag{17}$$

$$\left|\frac{2}{3}b_1^{(1,0)} + \frac{1}{3\sqrt{5}}b_1^{(1,2)} + 2\sqrt{\frac{2}{15}}b_3^{(1,2)}\right| \le \frac{2}{\sqrt{3}}\sqrt{\Delta}. \tag{18}$$

These equations involve three variables, at least one of which may possibly have a nonzero value (that is, is of the third kind) at $\beta = 2$. This is an important result for chirality detection at high photoelectron kinetic energies. The magnitude of these third kind of coefficients will be verified by numerical calculations.

However, because we have considered the necessary conditions, it is possible that the prefactors for Δ and $\sqrt{\Delta}$ are too large for a specific model. The validity of these equations was assessed by calculations using an explicit form of $b_L^{(K,k_\gamma)}$ as a function of bound-free transition dipole moments.

The coefficients $b_L^{(K,k_\gamma)}$ can be expressed in quadratic form based on bound-free transition dipole moments [41,53]. Therefore, an eigenvalue problem results [41,57] if we impose the appropriate normalization. Herein, we identify the maximum and minimum coefficients for Δ and $\sqrt{\Delta}$ by performing an eigenvalue analysis [53]. Table I shows the results obtained when including up to 10 or 40 angular momentum continuum states. It is evident that the values obtained in each case were within the range expected from the first and second cases. With respect to the first case, fortunately the maxima and minima obtained from the eigenvalue analyses were close to the expected upper and lower bounds, with a few exceptions, as seen in Table S1 in the Supplemental Material. The second category of parameters is restricted to a narrower range of 50–75%. This result is not unexpected because the number of coefficients $b_L^{(K,k_\gamma)}$ is larger than the number of transition dipole moments [41], and because we have only considered certain angles. Next, we examine the magnitude of coefficients at high energies by numerical calculations.

TABLE I. Upper and lower bounds of electronic factors. The numbers in the first column correspond to the equations (Eq.) in the main text. The second column provides the theoretical coefficients for $(2-\beta)$ and $\sqrt{2-\beta}$ for the first and second cases, respectively. The third and fourth columns show the maximum (minimum) coefficients obtained by eigenvalue analyses for which the highest angular momentum values ($l_{\max}$) are 10 and 40, respectively. Note that, in the case of analyses involving the first case, positive and negative eigenvalues were obtained separately and a $\pm$ symbol is added to indicate this.

Eq.	Theory	EVA	
	First case	$l_{\max} = 10$	$l_{\max} = 40$
(15)	$(1/\sqrt{6}) = 0.4082\cdots$	± 0.384	± 0.4062
(17)	$(1/\sqrt{6})$	± 0.399	± 0.4075
	Second case		
(16)	$(2/\sqrt{3}) = 1.1547\cdots$	0.837	0.8636
(18)	$(2/\sqrt{3})$	0.571	0.5769

PADs were calculated for hydrogen peroxide, methyloxirane, and camphor. The results for all molecules were similar. Those for hydrogen peroxide are presented in Fig. 3 while the methyloxirane results (Figs. S2 and S3) are provided in the Supplemental Material [53].

Within the Hartree-Fock approximation, the electronic configuration for hydrogen peroxide in its ground state, C_2 symmetry, is given by

$$(1a)^2(1b)^2(2a)^2(2b)^2(3b)^2(3a)^2(4a)^2(5a)^2(4b)^2, \tag{19}$$

based on nine occupied orbitals [Fig. 3(d)]. Calculations were performed for the equilibrium geometry as optimized

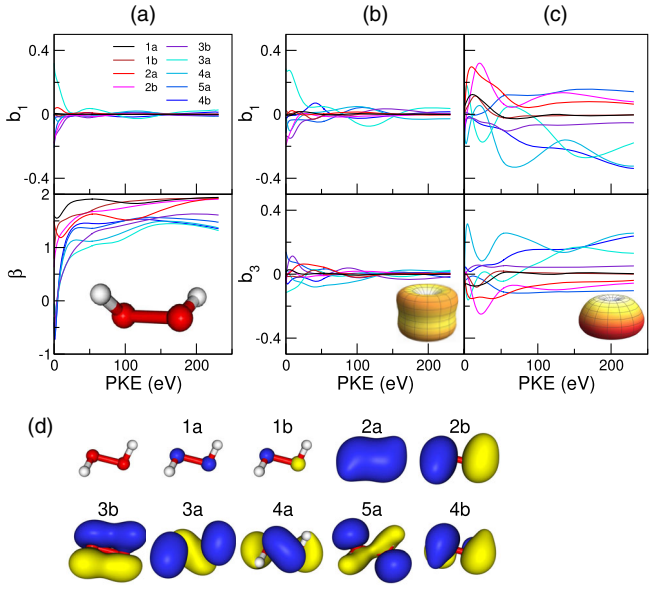

FIG. 3. H_2O_2 photoelectron anisotropy parameters for (a) one-photon ionization and resonant two-photon ionization assuming (b) $A_1 = 0$ and $A_2 = 2$ with circular polarization and (c) $A_1 = 1.5$ and $A_2 = 1$ with unpolarized light, as functions of the PKE. (d) Nine molecular orbitals for which these data were acquired. The insets to (b) and (c) show three-dimensional polar plots of the PADs for the $4b$ highest occupied molecular orbitals (HOMOs) at a photoelectron kinetic energy of 200 eV. Note that a dipole length operator was used to determine the bound-free transition dipole moments.

using the second-order Møller–Plesset perturbation theory with the 6-31G* basis set. Although hydrogen peroxide molecules are only chiral on a transient basis, it was assumed that each molecule adopted a single form with chirality. These calculations considered ionization from an initial orbital ϕ_0 to a continuum orbital with an effective one-electron potential [58,59]. The initial orbitals ϕ_0 were obtained by Hartree-Fock/4-31G calculations [Fig. 3(d)]. Continuum orbitals were obtained by the continuum multiple scattering $X\alpha$ method and were then orthogonalized with all orbitals occupied [58,59]. The alignment and polarization parameters were assumed to be at their maximum values of $A_2 = 2$ and $s_3 = 1$ for scheme (b) and $A_1 = 1.5$ with $A_2 = 1$ for scheme (c). In the case of two-photon ionization, the PAD was determined as

$$\frac{d\sigma}{d\Omega} = \sum_{L=0}^{4} b_L P_L(\cos\theta), \tag{20}$$

assuming that all photons were unpolarized or circularly polarized. Here, b_L are anisotropy parameters, and for one-photon ionization $b_1 = \sqrt{(3/2)}s_3 b_1^{(0,1)}$.

Figure 3(a) shows the calculation results for one-photon ionization using the dipole length form. These results reproduce the well-known trend in which, at higher energies, b_1 is close to zero and β is in the range of 1 to 2. The results obtained for two-photon ionization [Figs. 3(b) and 3(c)] confirmed that larger b_1 and b_3 values were associated with scheme (c) rather than with scheme (b), and that there were obvious differences in the three-dimensional polar plots of the PADs. The enhancement factor was also determined to be approximately 20 for the $4b$ HOMO in the vicinity of 200 eV.

In summary, the majority of coefficients for PADs were determined to be zero in the case that β is 2, due to the positivity of PAD; and effects of even-order molecular alignment [48,60] are expected to be small at high energies. Exceptionally, chirality-selective orientation [20,21,24,26] would be a powerful tool for chiral resolution by photoelectron recoil and for chirality detection in liquid samples [6–9], even if β is 2.

This work was supported by JSPS KAKENHI Grant No. 16K05665 from the Ministry of Education, Culture, Sports, Science, and Technology of Japan (MEXT).

*yoshiichisuzuki@hoku-iryo-u.ac.jp

[1] B. Ritchie, Theory of the angular distribution of photoelectrons ejected from optically active molecules and molecular negative ions, Phys. Rev. A **13**, 1411 (1976).
[2] N. A. Cherepkov, Circular dichroism of molecules in the continuous absorption region, Chem. Phys. Lett. **87**, 344 (1982).
[3] N. Böwering, T. Lischke, B. Schmidtke, N. Müller, T. Khalil, and U. Heinzmann, Asymmetry in Photoelectron Emission from Chiral Molecules Induced by Circularly Polarized Light, Phys. Rev. Lett. **86**, 1187 (2001).
[4] I. Powis, Photoelectron circular dichroism of the randomly oriented chiral molecules glyceraldehyde and lactic acid, J. Chem. Phys. **112**, 301 (2000).
[5] M. Tia *et al.*, Chiral asymmetry in the photoionization of gas-phase amino-acid alanine at Lyman-α radiation wavelength, J. Phys. Chem. Lett. **4**, 2698 (2013).
[6] S. Thürmer, R. Seidel, M. Faubel, W. Eberhardt, J. C. Hemminger, S. E. Bradforth, and B. Winter, Photoelectron Angular Distributions from Liquid Water: Effects of Electron Scattering, Phys. Rev. Lett. **111**, 173005 (2013).
[7] Y.-I. Suzuki, K. Nishizawa, N. Kurahashi, and T. Suzuki, Effective attenuation length of an electron in liquid water between 10 and 600 eV, Phys. Rev. E **90**, 010302(R) (2014).
[8] R. Signorell, Electron Scattering in Liquid Water and Amorphous Ice: A Striking Resemblance, Phys. Rev. Lett. **124**, 205501 (2020).
[9] S. Gozem, R. Seidel, U. Hergenhahn, E. Lugovoy, B. Abel, B. Winter, A. I. Krylov, and S. E. Bradforth, Probing the electronic structure of bulk water at the molecular length scale with angle-resolved photoelectron spectroscopy, J. Phys. Chem. Lett. **11**, 5162 (2020).
[10] D. Catone, M. Stener, P. Decleva, G. Contini, N. Zema, T. Prosperi, V. Feyer, K. C. Prince, and S. Turchini, Resonant Circular Dichroism of Chiral Metal-Organic Complex, Phys. Rev. Lett. **108**, 083001 (2012).
[11] G. Hartmann, M. Ilchen, P. Schmidt, C. Küstner-Wetekam, C. Ozga, F. Scholz, J. Buck, F. Trinter, J. Viefhaus, A. Ehresmann, M. S. Schöffler, A. Knie, and P. V. Demekhin, Recovery of High-Energy Photoelectron Circular Dichroism Through Fano Interference, Phys. Rev. Lett. **123**, 043202 (2019).
[12] Y.-I. Suzuki, A plane wave theory of photoionization using the dipole acceleration form: Predictions concerning circular dichroism in photoelectron angular distributions at high energies, J. Phys. B **53**, 215202 (2020).
[13] M. Ilchen, L. Glaser, F. Scholz, P. Walter, S. Deinert, A. Rothkirch, J. Seltmann, J. Viefhaus, P. Decleva, B. Langer, A. Knie, A. Ehresmann, O. M. Al-Dossary, M. Braune, G. Hartmann, A. Meissner, L. C. Tribedi, M. AlKhaldi, and U. Becker, Angular Momentum Sensitive Two-Center Interference, Phys. Rev. Lett. **112**, 023001 (2014).
[14] P. Decleva, D. Toffoli, R. K. Kushawaha, M. MacDonald, M. N. Piancastelli, M. Simon, and L. Zuin, Interference effects in photoelectron asymmetry parameter (β) trends of C $2s^{-1}$ states of ethyne, ethene and ethane, J. Phys. B **49**, 235102 (2016).
[15] H. C. Poon and S. Y. Tong, Focusing and diffraction effects in angle-resolved x-ray photoelectron spectroscopy, Phys. Rev. B **30**, 6211 (1984).
[16] S. Kono, Surface-structure analysis by forward scattering in photoelectron and Auger-electron diffraction and by backscattered primary electron diffraction, Surface Sci. **298**, 362 (1993).
[17] J. Cooper and R. N. Zare, Angular distribution of photoelectrons, J. Chem. Phys. **48**, 942 (1968).

[18] D. M. P. Holland, L. Karlsson, and K. Siegbahn, A reinvestigation of the vibrational structure and the orbital assignments in the photoelectron bands of cyclopropane, J. Electron Spectrosc. Relat. Phenom. **125**, 57 (2002).
[19] E. Hirota, Triple resonance for a three-level system of a chiral molecule, Proc. Jpn. Acad. Ser. B **88**, 120 (2012).
[20] D. Patterson and J. M. Doyle, Sensitive Chiral Analysis via Microwave Three-Wave Mixing, Phys. Rev. Lett. **111**, 023008 (2013).
[21] A. Yachmenev and S. N. Yurchenko, Detecting Chirality in Molecules by Linearly Polarized Laser Fields, Phys. Rev. Lett. **117**, 033001 (2016).
[22] A. A. Milner, J. A. M. Fordyce, I. MacPhail-Bartley, W. Wasserman, V. Milner, I. Tutunnikov, and I. S. Averbukh, Controlled Enantioselective Orientation of Chiral Molecules with an Optical Centrifuge, Phys. Rev. Lett. **122**, 223201 (2019).
[23] I. Tutunnikov, J. Floß, E. Gershnabel, P. Brumer, I. S. Averbukh, A. A. Milner, and V. Milner, Observation of persistent orientation of chiral molecules by a laser field with twisted polarization, Phys. Rev. A **101**, 021403(R) (2020).
[24] Y.-I. Suzuki, Wave packet simulations for molecular orientation induced by circularly polarized light: Toward chiral resolution in the gas phase, Chem. Phys. Lett. **785**, 139134 (2021).
[25] I. Tutunnikov, L. Xu, R. W. Field, K. A. Nelson, Y. Prior, and I. S. Averbukh, Enantioselective orientation of chiral molecules induced by terahertz pulses with twisted polarization, Phys. Rev. Res. **3**, 013249 (2021).
[26] L. Xu, I. Tutunnikov, Y. Prior, and I. S. Averbukh, Optimization of the double-laser-pulse scheme for enantioselective orientation of chiral molecules, J. Chem. Phys. **157**, 034304 (2022).
[27] I. Cacelli, V. Carravetta, A. Rizzo, and R. Moccia, The calculation of photoionisation cross sections of simple polyatomic molecules by L^2 methods, Phys. Rep. **205**, 283 (1991).
[28] K. L. Reid, D. J. Leahy, and R. N. Zare, Complete Description of Molecular Photoionization from Circular Dichroism of Rotationally Resovled Photoelectron Angular Distributions, Phys. Rev. Lett. **68**, 3527 (1992).
[29] K. L. Reid and J. G. Underwood, Extracting molecular axis alignment from photoelectron angular distributions, J. Chem. Phys. **112**, 3643 (2000).
[30] T. Seideman, Time-resolved photoelectron angular distributions as a probe of coupled polyatomic dynamics, Phys. Rev. A **64**, 042504 (2001).
[31] R. R. Lucchese, A. Lafosse, J. C. Brenot, P. M. Guyon, J. C. Houver, M. Lebech, G. Raseev, and D. Dowek, Polar and azimuthal dependence of the molecular frame photoelectron angular distributions of spatially oriented linear molecules, Phys. Rev. A **65**, 020702(R) (2002).
[32] Y. Suzuki and T. Seideman, Mapping rotational coherences onto time-resolved photoelectron imaging observables, J. Chem. Phys. **122**, 234302 (2005).
[33] A. G. Harvey, Z. Mašín, and O. Smirnova, General theory of photoexcitation induced photoelectron circular dichroism, J. Chem. Phys. **149**, 064104 (2018).
[34] V. L. Jacobs, Theory of atomic photoionization measurements, J. Phys. B **5**, 2257 (1972).
[35] J. C. Hansen and R. S. Berry, Angular distributions of electrons from resonant two-photon ionization of molecules, J. Chem. Phys. **80**, 4078 (1984).
[36] R. L. Dubs, S. N. Dixit, and V. McKoy, Circular-dichroism in photoelectron angular-distributions as a probe of atomic and molecular alignment, J. Chem. Phys. **85**, 656 (1986).
[37] K. L. Reid, D. J. Leahy, and R. N. Zare, Effect of breaking cylindrical symmetry on photoelectron angular distributions resulting from resonance-enhanced two-photon ionization, J. Chem. Phys. **95**, 1746 (1991).
[38] K. Bonhoff, S. Nahrup, B. Lohmann, and K. Blum, Angular distribution of molecular Auger electrons, J. Chem. Phys. **104**, 7921 (1996).
[39] S. Motoki, J. Adachi, K. Ito, K. Ishii, K. Soejima, A. Yagishita, S. K. Semenov, and N. A. Cherepkov, Complete photoionization experiment in the region of the $2\sigma_g \rightarrow \sigma_u$ shape resonance of the N_2 molecule, J. Phys. B **35**, 3801 (2002).
[40] A. N. Grum-Grzhimailo, On the angular distributions in molecular photoionization beyond the dipole approximation, J. Phys. B **36**, 2385 (2003).
[41] Y.-I. Suzuki and T. Suzuki, Determination of ionization dynamical parameters by time-resolved photoelectron imaging, Mol. Phys. **105**, 1675 (2007).
[42] Y.-I. Suzuki, Direct relation of molecular orbital symmetry with photoelectron angular distributions from aligned molecules in the gas phase, J. Phys. B **41**, 215204 (2008).
[43] C. N. Yang, On the angular distribution in nuclear reactions and coincidence measurements, Phys. Rev. **74**, 764 (1948).
[44] U. Fano and D. Dill, Angular momentum transfer in the theory of angular distributions, Phys. Rev. A **6**, 185 (1972).
[45] D. M. Brink and G. R. Satchler, *Angular Momentum*, 2nd ed. (Clarendon Press, Oxford, 1968).
[46] K. Blum, *Density Matrix Theory and Applications*, 2nd ed. (Plenum Press, New York, 1996).
[47] M. Tsubouchi, B. J. Whitaker, L. Wang, H. Kohguchi, and T. Suzuki, Photoelectron Imaging on Time-Dependent Molecular Alignment Created by a Femtosecond Laser Pulse, Phys. Rev. Lett. **86**, 4500 (2001).
[48] R. E. Goetz, T. A. Isaev, B. Nikoobakht, R. Berger, and C. P. Koch, Theoretical description of circular dichroism in photoelectron angular distributions of randomly oriented chiral molecules after multi-photon photoionization, J. Chem. Phys. **146**, 024306 (2017).
[49] R. L. Dubs, S. N. Dixit, and V. McKoy, Circular Dichroism in Photoelectron Angular Distributions from Oriented Linear Molecules, Phys. Rev. Lett. **54**, 1249 (1985).
[50] Y.-I. Suzuki, Y. Tang, and T. Suzuki, Time-energy mapping of photoelectron angular distribution: Application to photoionization stereodynamics of nitric oxide, Phys. Chem. Chem. Phys. **14**, 7309 (2012).
[51] J. B. Williams, C. S. Trevisan, M. S. Schöffler, T. Jahnke, I. Bocharova, H. Kim, B. Ulrich, R. Wallauer, F. Sturm, T. N. Rescigno, A. Belkacem, R. Dörner, T. Weber, C. W. McCurdy, and A. L. Landers, Imaging Polyatomic Molecules in Three Dimensions Using Molecular Frame Photoelectron Angular Distributions, Phys. Rev. Lett. **108**, 233002 (2012).
[52] E. Plésiat, P. Decleva, and F. Martín, Relationship between polarization-averaged molecular-frame photoelectron

angular distributions and geometry, Phys. Rev. A **88**, 063409 (2013).

[53] See Supplemental Material at http://link.aps.org/supplemental/10.1103/PhysRevLett.130.143202 for a full list of parameters of the first and second kinds, with their detailed derivation, and details of the eigenvalue analysis, including additional figures for nitrogen and methyloxirane and Refs. [58–60].

[54] R. N. Zare, *Angular Momentum: Understanding Spatial Aspects in Chemistry and Physics* (Wiley, New York, 1988).

[55] R. L. Dubs, S. N. Dixit, and V. McKoy, Circular-dichroism in photoelectron angular-distributions as a probe of atomic and molecular alignment, J. Chem. Phys. **86**, 5886 (1987).

[56] A. Szabo and N. S. Ostlund, *Modern Quantum Chemistry: Introduction to Advanced Electronic Structure Theory* (Dover, New York, 1996).

[57] W. Thiel, Theoretical analysis of phtoelectron angular distributions of linear molecules, Chem. Phys. **77**, 103 (1983).

[58] D. Dill and J. L. Dehmer, Electron-molecule scattering and molecular photoionization using the multiple-scattering method, J. Chem. Phys. **61**, 692 (1974).

[59] Y.-I. Suzuki and T. Suzuki, Photoelectron angular distribution in valence shell ionization of heteroaromatic molecules studied by the continuum multiple scattering Xα method, J. Phys. Chem. A **112**, 402 (2008).

[60] S. Beaulieu, A. Comby, D. Descamps, S. Petit, F. Légaré, B. Fabre, V. Blanchet, and Y. Mairesse, Multiphoton photoelectron circular dichroism of limonene with independent polarization state control of the bound-bound and bound-continuum transitions, J. Chem. Phys. **149**, 134301 (2018).